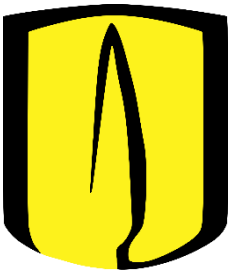

UNIVERSIDAD DE LOS ANDES

ELECTRIC AND ELECTRONICS DEPARTMENT

GRADUATION THESIS DEGREE IN ELECTRONICS ENGINEERING

MICROHEATER FOR MICROFLUIDICS SYSTEMS

Presented by
LUISA FERNANDA FUENTES MELO

Advisor
JOHANN F. OSMA

Co-advisor
CRISTIAN F. RODRIGUEZ
SANTIAGO TOVAR

Judge
DIANA SOTELO

BOGOTÁ-COLOMBIA
December 2022

Lf.fuentes@uniandes.edu.co

Article

Microheater for microfluidics systems

Luisa Fernanda Fuentes Melo [1, *]

[1] Biomicrosystems, Department of Electrical and Electronics Engineering, School of Engineering, Universidad de los Andes, Cra. 1E No. 19A-40, Bogota 111711, Colombia ; * lf.fuentes@uniandes.edu.co

Abstract: Microfluidics devices have been a tool to develop low-cost alternatives for research in pharmaceutical, medical, and biomedical fields. This is because they allow miniaturizing the process and thus reduce the volumes of reagents needed. However, one of the most challenging variables to control within low-cost microfluidic devices is temperature due to the high costs of microheaters for microfluidic devices since they are manufactured in a clean room. This is why the need arises to simulate, design, and test a low-cost microheater that can be coupled to microfluidic devices. Electro-Thermal-Mechanical mathematical model was proposed in the COMSOL Multiphysics 6.0® software (COMSOL Inc., Stockholm, Sweden), which allowed an extensive study of different geometries for the microheater, allowing for varying both the number of turns of the microheater (m and n) and the distance between turns (w). After determining the optimal geometry with in silico studies, the micro heater was manufactured and characterized using an infrared thermometer and a thermal camera. The characterization determined an operational range for the microheater between 1v to 12v to reach temperatures between 25°C to 120°C. The simulations presented an error concerning the experimental results of 10.99955% with the Infrared Thermometer and 14.75182% with the Thermal Camera.

Keywords: Microheater, Microfluidic systems, Heat control, Thermal characterization, Electrothermal system, Control system.

Citation: To be added by editorial staff during production.

Received: date
Accepted: date
Published: date

1. Introduction

1.1. Microfluidics systems and Microheater

Microfluidics is the science of manipulating fluids in channels at the microscale and nanoscale [1]. This technology has considerably spread in recent years due to its diverse applications in chemistry, biology, medicine, physical sciences, and electronics, among others [2]. One of the most significant contributions of this field is the development of lab-on-chip (LOC) devices, which is expected to generate a revolution in chemistry and biology since such devices can integrate entire laboratories on a single chip. This is achieved due to the design of microfluidic channels and components such as filters, valves, and mixers, among others [2]. The advantage of this technology is its ability to manage small fluid samples, which allows analysis with a small number of fluids. Likewise, these systems significantly reduce the number of reagents needed in the processes, which positively impacts the environment and allows for measurement automation.

Since heating is an essential process in science and engineering, a considerable amount of work has been done on the miniaturization of heaters to enable efficient operation in remote locations. In addition, microheaters have the advantages of reduced power consumption and volume, improved thermal response, and easier integration into microfluidic sensors or chips [3]. Although different elements can generate heat, such as induction, infrared, or microwave waves, in this article we will focus mainly on electrical radiation.

The first research on resistive heating was done by James Prescott Joule in 1841. However, his method was only confirmed once Michael Faraday presented his findings in 1849 when he achieved recognition from the Royal Society of London [4]. The main goal of a microheater is to establish a suitable heating environment with precise temperature

control for the microfluidic device [3]. In addition, the downscaling of heaters results in reduced thermal mass and power consumption, resulting in faster response times and higher temperatures as well as the generation of battery-powered technology [5]. The design of the resistive microheater is because temperature depends on physical, mechanical, and thermal factors, in addition to material properties and geometric design [6].

1.2. Materials

Microheaters are generally made of conductive materials such as platinum (Pt), gold (Au), silver (Ag), Nichrome (Nicer), Titanium (Ti), Aluminum (Al), Copper (Cu), or graphene [7] .The materials' electrical resistivity should be high compared to the substrate so that efficient Joule heating occurs in the heater resistance and unwanted heat in the contact pads can be reduced [3]. According to the literature, platinum is the best material to design heaters and sensors since it features lower density, good heat capacity, high thermal conductivity, low energy consumption, and linear change between resistance and temperature in addition to being a dense, malleable, and less reactive material. However, this material has the problem that it is not possible to deposit it on the glass substrate, so it is necessary to have a layer of Titanium or Chromium to improve the adhesion of the material [8]. Another material that is used in the manufacture of microheaters is Nichrome, which in literature is reported as a suitable material due to its electrical resistivity, high thermal conductivity, and coefficient of resistance at low temperatures but stability at elevated temperatures and does not require platinum, a layer with adhesive elements which makes the sensor and heater more cost-effective [9]. Finally, among the efficient metals for these applications are Aluminum and Copper. Since aluminum has an oxide layer, the best choice is copper due to its good linearity, low cost, and excellent electrical and thermal conductivity [10].

Table 1. Physical, mechanical, electrical, and thermal characteristics of various microheater materials [3]

Materials	Electrical Properties		Thermal Properties			Mechanical Properties	
	Resistivity at 20°C (ohm/m)	Electrical conductivity (S/m)	Specific heat (J/Kg K)	Thermal conductivity (W/mk)	Thermal Expansion Coefficient at 20 °C × 10–6 (°C–1)	Young's Modulus (GPa)	Yield Strength (MPa)
Ag	1.59 × 10–8	6.30 × 107	234	419	18	76	55
Al	2.65 × 10–8	3.77 × 107	900	210	23.1	68	11
Au	2.44 × 10–8	4.11 × 107	128	301	14	77.2	205
CNT	1 × 10–6	106 to 107	600	210	15.4	270—950	-
Cr	12.5 × 10–8	7.9 × 106	461	93.9	4.9	279	250
CrN	300 × 10–6	3.33 × 103	-	19.25	9.4	200	-
Cu	1.68 × 10–8	5.96 × 107	385	398	17	110	33.3
Ni	6.99 × 10–8	1.43 × 107	460	60.7	13	207	59
NiCr	1.10 × 10–6	6.70 × 105	450	11.3	14	220	344.73
Pt	1.06 × 10–7	9.43 × 106	134	69.1	9	-	180
SiC	202 × 10–8	0.7–1.4 × 102	670	180–250	11	410	21 GPa
Sn	1.09 × 10–7	9.17 × 106	256	60.7	4.7	44.3	11
SnO2	2–4 × 10–5	5 × 104	44.3 J/mol K	98	4	280.59	-
Ta2O5	1.92 × 10–6	5.2 × 105	-	5	3.25	62.7	-
Ti	4.20 × 10–7	2.38 × 106	528	17	8.6	116	140
W	5.60 × 10–8	1.79 × 107	134	163.3	4.5	400	750

1.2.1. Design and Geometry

The design and material of the microheater are fundamental to enable low energy consumption, low thermal mass, temperature uniformity, and better thermal insulation with the surroundings [11]. Decreasing the thickness of the microheater would increase

the resistance, thus reducing energy consumption and heating temperature. The equation (1) gives the micro-heater resistance:

$$R = \frac{pl}{A} \quad (1)$$

R is the resistance at the same temperature where it is specific, p is the material's resistivity , l is the length of the resistor, and A is the resistor's cross-sectional area (width x thickness). However, the design of the microheater can vary according to the application, from simple line patterns to complex patterns that guarantee uniform thermal distribution [3]. Likewise, it should be considered that in multiple applications more than one microheater should be used; for example, for molecular and cellular analysis in a polymerase chain reaction (PCR), glucose analysis, enzymatic behavior analysis, DNA analysis, cell manipulation using thermosensitive polymers, among others [6]–[8]

1.3. Control module

Although the design processes, choice of materials, and geometry are essential, implementing an efficient temperature controller is decisive for uniform thermal distribution in the microheater. For example, in research, a feedback control algorithm was developed that achieved a constant temperature distribution [12]. Given this, it can be concluded that the control module is critical to maintaining the temperature on the microheater surface by applying the desired voltage, as shown in Figure 1; this should comprise a sensor that detects the microheater temperature, a control system with a dedicated algorithm to calculate the desired voltage requirements, and an-output microcontroller that delivers the corresponding voltage to the microheater [3]. Based on thermal performance investigation, it was found that the heater can perform its job effectively in the microchannel air flow without any significant increase in on-chip temperature. If fluid flows through the microchannel, the heater temperature decreases with an increased flow rate [13]. This can be improved by optimizing the distribution of the heating power density around interest [14].

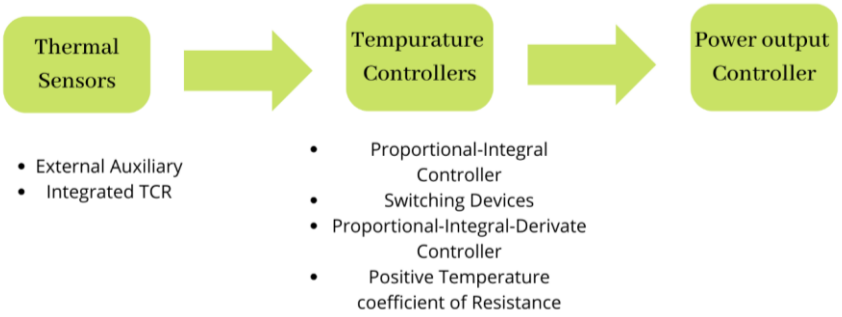

Figure 1. The process involved in automatic temperature control [3]

1.4. Thermal sensors

The thermal sensor is one of the main components to detect and supply information to feed back to the control module. This part facilitates the temperature distribution by providing the heater according to the required device's requirements and portability. This leaves the option of employing this technology internally or externally [3]. In the early days of thermal sensing, the analysis was performed using external equipment such as an infrared (IR) camera. However, with the advent of modern technology, these aids have been used mainly to calibrate and analyze the heating pattern of the microheater. In addition, it helps microscopic monitoring of cellular activities such as cultures which could end up with the elimination of conventional incubators; for example, in research, a transparent ITO microheater device with dedicated temperature control was developed [15]. Similarly, in another study, a method was developed to measure the temperature of the microheater using an IR microscope, allowing us to conclude that different widths in atmospheric conditions and deionized water do not significantly affect the temperature [16];

the problem with these conventional measurements is that they increase costs, generate more significant inaccuracy in the model and limit the portability of the device compared to integrated sensors [17].

On the other hand, the integrated sensors can change the resistance depending on the temperature within the range, which helps to detect the temperature once the system is calibrated. The cost and fabrication of such sensors can be reduced by using similar materials as the micro heater. An example of this is found in the research study where Pt sensors were fabricated and integrated into gas microsensors for thermal measurement and control. For sensor calibration, they focused on the correlation of the electrical resistance change with applied power and temperature increase [18]. Later, in another research, a four-point TCR probe was developed in a microheater based on AG and Ti featuring a double spiral geometry on a glass substrate to supply Joule heating current and detect voltage drops. This structure delivered 60°C with a power consumption of 210 nW [19]. The power consumption and resistance characteristics depend on the temperature of the microheater, which, as reviewed in the literature, can be measured by the 4-point method. This method is beneficial since it accurately figures out the voltage applied to the heater and uses a time-of-flight speed sensor of the microheater [20], [21].

1.5. Temperature control systems

Electric heaters have been shown to require more time to reach higher steady-state temperatures, but this time can be reduced by initially driving a higher voltage to get to the specified limit. Once this limit is achieved, the desired voltage is set to keep the steady-state temperature [22]. Still, this technique has been found to reduce thermal accuracy since the resistance varies as a function of time and temperature. Additionally, it has been shown that simulation by the finite element method is necessary to predict the voltage needed to drive the heater, but periodic temperature control is still required [3]. Some of the control systems reported in the literature were switching systems, proportional-integral (PI) controllers, and proportional-integral-derivative (PID) controllers; in addition, a positive temperature resistance coefficient can be applied to derive external devices, which makes the system more portable and economical [3].

The first control is the closed-loop feedback control with an on/off function since it is the most economical system and offers a temperature rise time close to 1.5s. This control first supplies the maximum energy to increase the temperature of the microheater until it is lower than the set point [3]. A case of this can be seen in the development of a project where a pulse width modulator (PWM) signal was used for the output regulator module to allow the temperature to be controlled so that this control module turned the voltage output on and off to supply the desired temperature [23] [24]. Further, a control system was designed employing an AT-Mega 8535 circuit, a signal conditioner, a current controller, LCD, RS-232 serial communication, and the micro heater. This employed PWM method was adopted to have minimum power loss in the switching devices by a transistor controlling the output current, resulting in temperature control with high stability and short delay and settling period [25]. Subsequently, an advanced thermal cycle controller based on a touch module for a dual heater using PWM was provided in an investigation; this generated that the temperature, time, and the number of cycles of the PCR were automated by the touch screen [26]. Finally, a micro heater integrated with a micro thermal sensor and a cooling channel was developed for higher speed and reduced PCR test time [27].

The second type of controller found is the proportional-integral (PI), which avoids temperature oscillations by easing a slow temperature rise while reaching the reference temperature resulting in an average of 7.6 s [3]. Subsequently, in development for low-temperature applications, an aluminum microheater was developed with an integrated nickel thermal sensor with a closed loop temperature control for faster response obtaining results of 1.5 s faster than ordinary PI controllers [28]. Some further improvements seen in the literature is the development of an open-loop to closed-loop switched proportional-integral (OLCLS PI) control that combines both control strategies, initially behaving as an

open loop for a shorter rise time and then switches to a closed-loop control which improves the controller response being even faster than a PID controller and has a comparable disturbance handling to a PI [29].

The third type of control employed is PID; this includes proportional, integral, and derivative actions. Proportionate actions produce control proportional to the error. Integrals eliminate stationary error, and derivatives decrease overshoot and introduce damping [30]. The PID circuit has a similar feedback and connection circuit with parallel cabling minus the latching relay circuit; however, in principle, it retrieves the temperature data and feeds the PID, which decides the drift error by controlling and calculating the output signal. PWM was employed to achieve a constant output signal since it supplies good control accuracy as in the PID, but it does not require any adjustment every time the setpoint values are changed [31]. Later, an electronic circuit was developed based on earlier research [32] and performed temperature control using a PID algorithm where the electronic board drives the microheater and compares the voltage of a morphos silicon diode with its setpoint temperature until the reference is reached [33]. Then, a microcontroller based on a temperature plate was specially designed to control and read the DACs and ADCs and communicate with a computer where the PID control circuit software was installed [34]. This interface was subsequently upgraded to allow the user to manage, edit and control basic biochemical protocols. A local host with a PIC18F4550 microcontroller was adapted; this system senses the temperature every 5ms and calculates the output signal via PID [35]. For applications such as MAPS, it was necessary to have precise temperature control to reach 400°C in 1ms. Therefore, a closed-loop control based on the temperature-resistivity relationship was developed by employing an 8-bit Arduino Mega as a microcontroller, which calculated the microheater resistance and varied the voltage input [36]. Like the above, in DNA amplification applications, in one investigation, it was possible to generate the temperatures needed to denature, band, and extend the genetic material using a control system on a Cortex-M3 ARM microcontroller based on a fuzzy PID with PWM to regulate the power of the microheater [34].

Finally, a positive temperature coefficient of resistance (PTCR) control system is reported in the literature. It is based on implementing automated resistive heating elements that can maintain preset temperatures without needing electronic regulation systems, thus improving their portability in applications. These materials allow for a rapid increase in resistance at elevated temperatures; for example, if it is PTC polymer-based, it takes 5 min to reach the set temperature of 61.5 ± 64°C and holds up to 25 min [36]. This approach was simple, economical, and did not need any control system. However, these materials have the problem of taking a long time to reach the desired temperature and are not ideal for processes where several cycles are needed.

1.6. Objetives

Design, simulate, and test a low-cost microheater with temperature control to suit different applications in microfluidic systems

- Design and simulate a resistor that allows the device to remain at temperatures suitable for the processes
- Perform the corresponding simulations to verify that the process control, time, and temperature are adequate for both the heater and the microfluidic system.
- Verify the results obtained, document the characteristics of use for future applications in microfluidics.

2. Materials and Methods

2.1. Materials, Equipment and Software

Analysis simulations were implemented under a thermal-electrical-mechanical study in COMSOL Multiphysics 6.0® design software (COMSOL Inc., Stockholm, Sweden). Then ALTIUM DESIGNER system engineering software (Altium Limited, Australia) was used to design and generate the selected geometry in a GERBER circuit printout file. Another necessary software was MATLAB Online (MathWorks, Natick, Massachusetts, USA) to find the transfer functions of the microheater.

The materials used in the design and manufacture of the microheater were fiberglass reinforced epoxy resin, also known as FR4 (Microcircuitos, Cali, Colombia), as the base of the printed circuit and a 99.99% pure copper layer (Kurt J. Lesker Company, Clairton, PA, USA) with a cross-sectional area of 35 micrometers for the PCB tracks. For the manufacturing process, the following equipment was necessary: Photoengraver (FILMSTAR-PLUS Bungard, Windeck, Germany), perforator (CCD/2 Bungard, Windeck, Germany), laminator (LAMINA-TOR RLM 419P Bungard, Windeck, Germany), insolator (HELLAS Bungard, Windeck, Germany), etcher (HELLAS Bungard, Windeck, Germany), etchant (HELLAS Bungard, Windeck, Germany), etching machine (HELLAS Bungard, Windeck, Germany), Windeck, Germany), spray etcher (SPLASH CENTER Bungard, Windeck, Germany), a through hole plater (COMPACTA L30 ABC Bungard, Windeck, Germany) and finally an optical verification and guillotine cutting of the printed circuit board was performed.

A Portek DF1731SB3A variable voltage source (Proteck Electronics Corp, China), PeakTech Multifunction Tester® 3725 digital multimeter (PeakTech Prüf und Messtechnik GmbH, Ahrensburg, Germany), a PeakTech 4950 infrared thermometer (PeakTech, Hamburg and Lübeck, Germany) and a Raspberry Pi4 (Adrafruit Industries, Hamburg and Lübeck, Germany) were required for the supply and measurements in the characterization process, Ahrensburg, Germany), a PeakTech 4950 infrared thermometer (PeakTech, Hamburg and Lübeck) and a Raspberry Pi4 (Adrafruit Industries, New York City, USA) controlling the MLX90640 thermal camera (Adrafruit Industries, New York City, USA). USA).

The design dimensions were the same as those of most microfluidic systems manufactured by the Biomicrosystems research group of the Universidad de Los Andes. These were 2.5 cm wide and 7.5 cm long. For the width of the circuit tracks, we took the recommendation of the staff of the printed circuit laboratory of the Universidad de Los Andes, and they were designed with 0.2 um, which is the minimum design that can be done in the laboratory to avoid printing problems or discontinuities in the circuit and a cross-sectional area of the conductive material (copper) of 35 micrometers. The general process for the modeling and design of the microheater is illustrated in Figure 1.

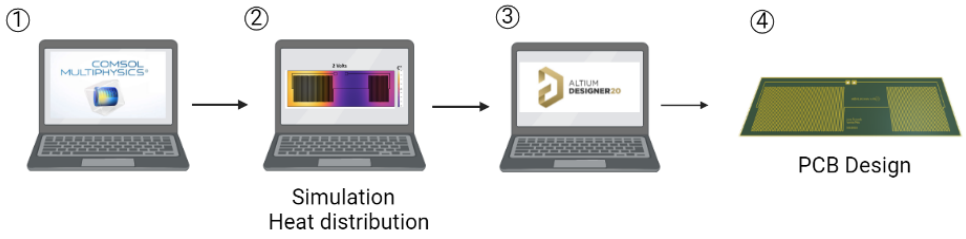

Figure 1. General design and simulation process of the microheater for fluidic systems. (1) COMSOL Multiphysics 6.0® software was used to simulate the chosen geometry with the corresponding materials of the FR4 glass substrate and the conductive material Copper. (2) Simulation results of the temperature distribution on the microheater surface at different voltage values. (3) Design of the selected geometry in ALTIUM DESIGNER software. (4) Generation of GERBER files to print the circuit (PCB).

2.2. Modeling of the Microheater

The microheater was studied using an Electro-Thermal-Mechanical mathematical model in the COMSOL Multiphysics 6.0® software (COMSOL Inc., Stockholm, Sweden).

The heat transfer in the microsystem was governed by the heat transfer equation (2).

$$\rho C_\rho U \cdot \nabla T + \nabla \cdot q = Q_{ted} + Q (2)$$

Where ϱ is the density, C_ρ is the heat capacity, U is the velocity vector of translational motion, T is the temperature, q is the heat flux by conduction, Q is the heat generated by the circuit, and Q_{ted} is the thermoelastic damping described by equation (3).

$$Q_{ted} = -\alpha T \frac{ds}{dt} (3)$$

Where α is the coefficient of thermal expansion, and S is the second Piola-Kirchhoff tensor. The microheater was modeled as a thin layer to reduce the computational cost. This approximation generates an extra dimension that is a 1D line representing the multiple layers in the thin structure, the heat transfer in this thin layer is governed by equations (4).

$$-n \cdot q = d_s Q_s - \nabla_t \cdot (d_s q_s) (4)$$

Where n is the normal vector, q is the conductive heat flux vector, the shell thickness is the microheater's heat source, and the solid conductive heat flux is described by equation (5).

$$q_s = -k \nabla_t T (5)$$

Where k is the micro heater's thermal conductivity, the micro heater's electric current is governed by Ohm's law (6).

$$J = \sigma E (6)$$

Where is the electrical conductivity, is the current density, and is the electrical field described by equation (7).

$$E = -\nabla V (7)$$

Where V is the electric potential. The power density in the microheater was governed by equation (8)

$$P_d = J \cdot E (8)$$

The heater rate per unit is governed by equation (9), the coupled parameter in equation (1).

$$Q = P_d \cdot d_s (9)$$

The deformation of the acrylic microchannel was studied using a total Lagrangian formulation, in which the equation of motion governs the mechanical behavior in the microchannel. (10).

$$0 = \nabla \cdot s + F_v (10)$$

Where F_v is the volume force vector, s is the stress the second Piola-Kirchhoff stress. By assuming geometrically linear analysis, the Green-Lagrange strain becomes equation (11)

$$\varepsilon = \frac{1}{2}(\nabla U^T + \nabla U) (11)$$

Where U is the structural displacement vector. In particular, the thermal stress is governed by equation (12)

$$\varepsilon_{\text{th}} = \alpha(T - T_r) (12)$$

Simulations to solve the Electro-Thermal-Mechanical mathematical model equations were conducted via a Stationary study with a MUMPS solver. The computational domain meshed with 71817 domain elements, 48247 boundary elements, and 6341 edge elements (Figure 2). These meshing levels allowed convergence. The boundary conditions to solve the model were the ground and the circuit's electric potential. In addition, the heat fluxes with the air at the edge of the microdevice. The boundary conditions for the simulations are shown in Figure 2.

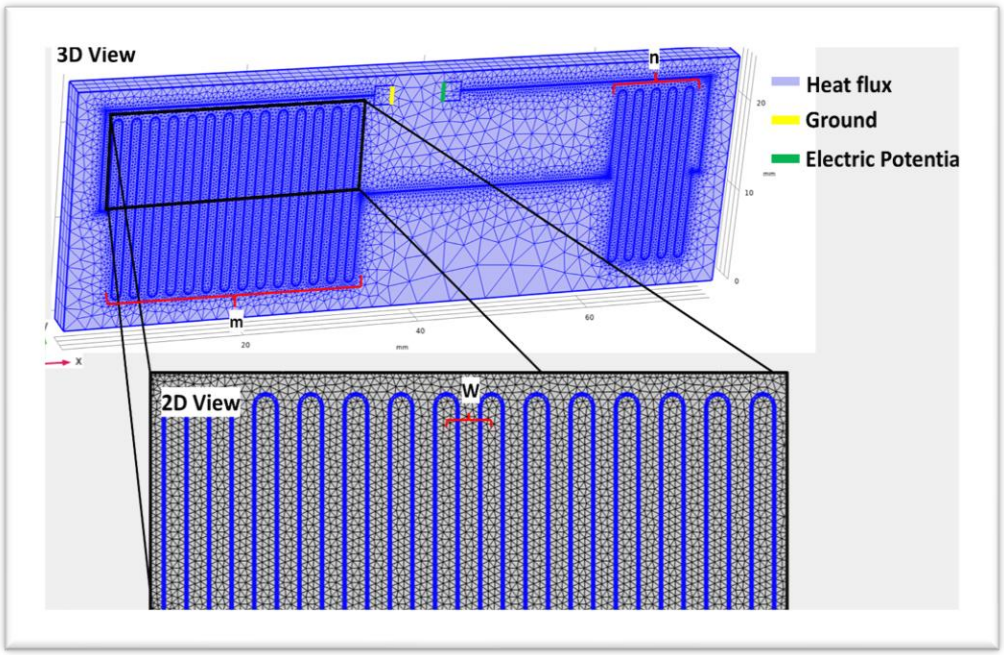

Figure 2. Boundary conditions for the simulations. The ground in the circuit is shown in yellow, and the electric potential is shown in yellow. The heat flux with air was applied to the contours of the microdevice; the air was assumed to be 20 C° .m is the number of loops that resistance 1 has, n is the number of loops that resistance 2 has, and w is the distance between loops.

The mathematical model assumed a copper resistance for the micro heater and an acrylic (PMMA)microfluidic device. Table 2 shows all the simulation parameters.

Table 2. Microheater simulation parameters [3], [37]

Materials	Property	Value
Copper	Thickness	35 [um] [Tovar]
	Relative permittivity	1
	Heat capacity	100 [J/(kg*K)]
	Density	8960 [kg/m^3]
	Rotation	0.0 deg
	Young´s modulus	110e9 [Pa]
	Poisson´s ratio	0.35
	Thermal conductivity	100 [W/(m*K)]
	Electrical conductivity	5.96e7 [S/m]
	Coefficient of thermal expansion	17e-6 [1/K]
	Mesh elements	5
FR4	Coefficient of thermal expansion	0.55e-6 [1/K]
	Heat capacity	250 [J/(kg*K)]
	Density	2203 [kg/m^3]
	Thermal conductivity	1.059 [W/(m*K)]
	Young´s modulus	73.1e9 [Pa]
	Poisson´s ratio	0.17

Mainly in this design, the temperature was distributed in three different spaces on the surface of the microheater by changing the parameter of the number of turns of the coil. In this way, we could ensure the presence of three different temperatures for multiple applications requiring or wishing to operate under different conditions as shown in Figure 3.

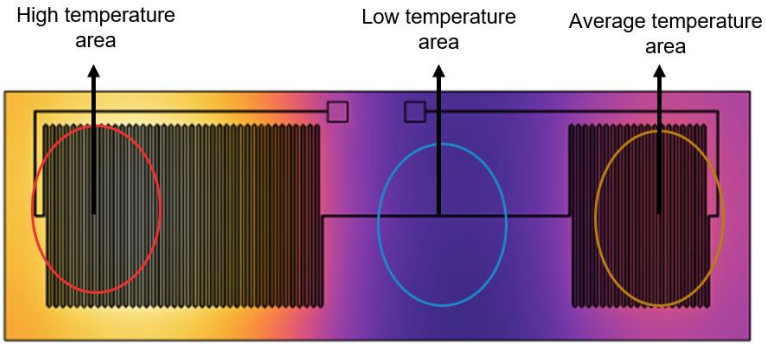

Figure 3. Temperature distribution over the surface of the microheater and indication of the highest, lowest, and middle temperature zone of the microheater.

When the simulations were as desired, we proceeded to extract the geometry from the COMSOL Multiphysics 6.0® software in a DXF format to enter it into the ALTIUM DESIGNER 2.0 software where the PCB would be designed. It was necessary to use polygons and lines to complete the geometry on the PCB and to add pads where the holes for the connectors that would be added later would be drilled.

2.2. PCB Manufacture

The PCB manufacturing process continued after the geometry was established in the ALTIUM DESIGNER 2.0 software and the PCB GERBER files were generated. The manufacturing procedure is shown in Figure 4.

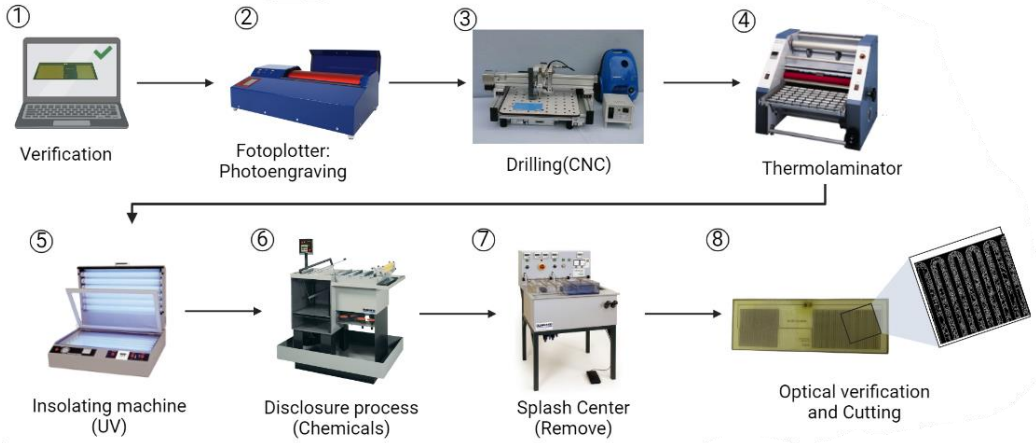

Figure 4. General process of microheater manufacture.

The manufacturing process begins with verifying the GERBER files generated in the ALTIUM DESIGNER 2.0 software. For this, it is necessary to satisfy all the minimum standards and conditions required by the laboratory to design a printed circuit that works properly. Secondly, the photo engraving process (photoplotter) is the technique that allows printing using a red laser light beam to the negative or positive transparencies of the designs on the photosensitive film (Helium-Neon film) to the red laser, this photographic process is performed in the darkroom, and chemical products are used with developer and fixer. It is appropriately washed to remove traces of the products and dry the design. Thirdly, the drilling process (CNC) is performed, which consists of drilling the perforations or vias present in the printed circuit, the position, and diameter of which must already be indicated in the file. Fourthly, the thermolaminating process is performed with

pressure, temperature, and speed adjustment with a roll of photosensitive film on the FR4 substrate.

Subsequently, a double-sided insolator is used in the fifth place, a vacuum UV light exposure chamber that allows the PCB design to be transferred to the FR-4 substrate presensitized with a double-sided photosensitive film. Sixth, the etching process is carried out using a Splash Center. This machine performs the double-sided spraying process with temperature and pressure control, releasing corrosive agents such as ferric chloride to eliminate the excess copper from the substrate. In the seventh step, with the same equipment mentioned above, the etched photosensitive film is removed from the design with a chemical process. Finally, an optical verification of the circuit is carried out using a microscope to check that there are no shorts, open tracks, or perforations without copper covering to guarantee the operation of the design. Then a guillotine is used to cut the size or shape of the design requested by the user. This whole process was carried out in the Universidad de Los Andes printed circuits laboratory with the help of laboratory technician Alejandro Monroy Ocasiones.

2.3. Microheater Characterization

Different processes were carried out to characterize the microheater. First, we calculated the resistance´s theoretical and practical value to determine if the final product complied with the design conditions. For this, equation (1) was necessary, which indicates the corresponding resistance depending on the conductive material´s resistivity coefficient, the resistance´s total length, and the cross-sectional area. A PeakTech Multifunction Tester® 3725 digital multimeter was used to determine the resistance of the printed circuit board. Figure x6 shows the general characterization process of the microheater.

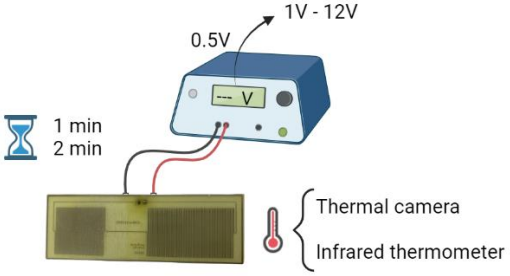

Figure 5. General characterization process of the microheater with voltage variations of 0.5 in a range of 1 volt and 12 volts. Measurements were taken every minute and two minutes from the voltage input with two different temperature measurement methods, an infrared thermometer, and a thermal camera.

Two different techniques were used to characterize its operation: An infrared thermometer and a thermal camera, always in the area with higher temperatures, as shown in Figure x2. The resistance was connected to a variable voltage source and began to take the temperature at 1 minute and 2 minutes from its connection, varying the input voltage starting at 1 volt and going up by 0.5 volts until reaching 12 volts. This process was repeated 3 times with the same resistor and 2 different resistors to ensure similar behavior in each design and the replicability of the microheater. This process resulted in the characteristic curves of the system.

As the last process, the time versus resistance verification test was performed to determine how long the microheater needed to stabilize the temperature. The highest temperature recorded in the previous process with its corresponding voltage was chosen, and temperature measurements were taken every 30 seconds with the same two methods for 6 minutes. It was replicated 3 times with the same resistance to verify how the system achieves stability and calculate its transfer function to design a control system. In Figure 6 we can observe the assemblies corresponding to the temperature characterizations with both methods.

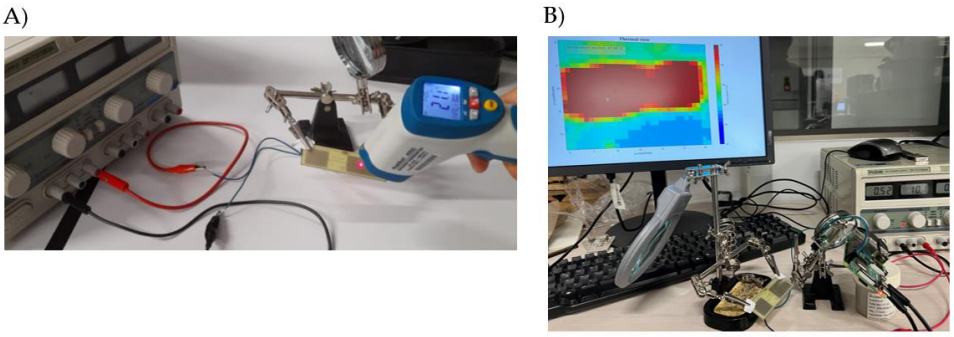

Figure 6. Assemblies of both characterizations A) with the PeakTech 4950 infrared thermometer and B) with the MLX90640 thermal camera.

3. Results and Discussion

3.1. Model of the Microheater

The mesh convergence study of the Electro-Thermal-Mechanical model is presented in Figure 7, which shows the convergence with 48111 domain elements, 9663 boundary elements, and 2314 edge elements. The convergence was evaluated with point evaluation for the temperature in the center of the microheater. For this mesh, boundary layers with a thickness adjustment factor of 1.0 and a stretching factor of 0.4. All the subsequent studies were carried out with this mesh discretization.

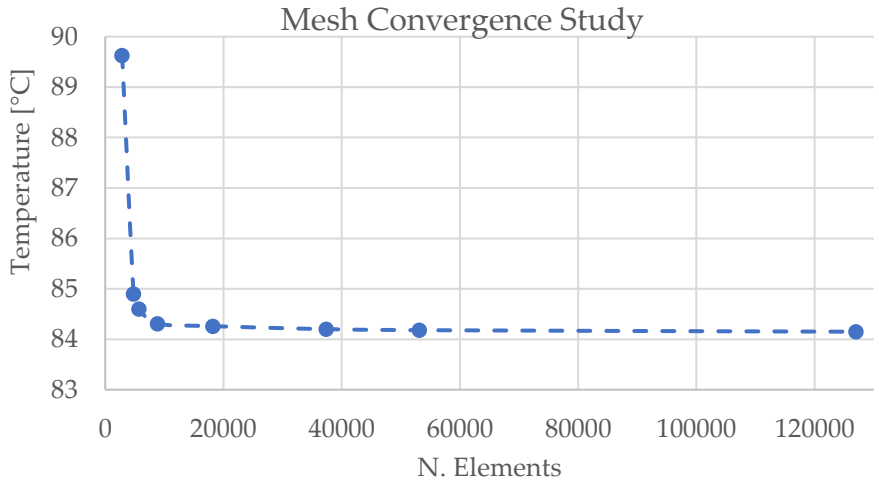

Figure 7. Mesh convergence study of the model with stability in 48111 *domain* elements, *9663 boundary elements, and 2314 edge elements.*

Figure 8 shows the microheater's temperature results by varying the microheater's geometry. Simulations show that decreasing the distance between loops (W) condenses the temperature in some regions of the micro heater. One of the applications of the micro heater is to serve as a platform to carry out temperature screening tests. Therefore, the value of separation distance between loops (w) was selected, allowing three zones of established and homogeneous temperatures over which microchannels could pass. In silico studies were used to analyze many geometries, varying the number of loops, which had both the resistance on the left (m) and the resistance on the right (n). Increasing the turns generates an increase in resistance and therefore decreases the temperature. The combination of the number of loops of the resistance on the left (m) and the resistance on the right (n) which the desired temperatures for temperature screening are achieved was determined.

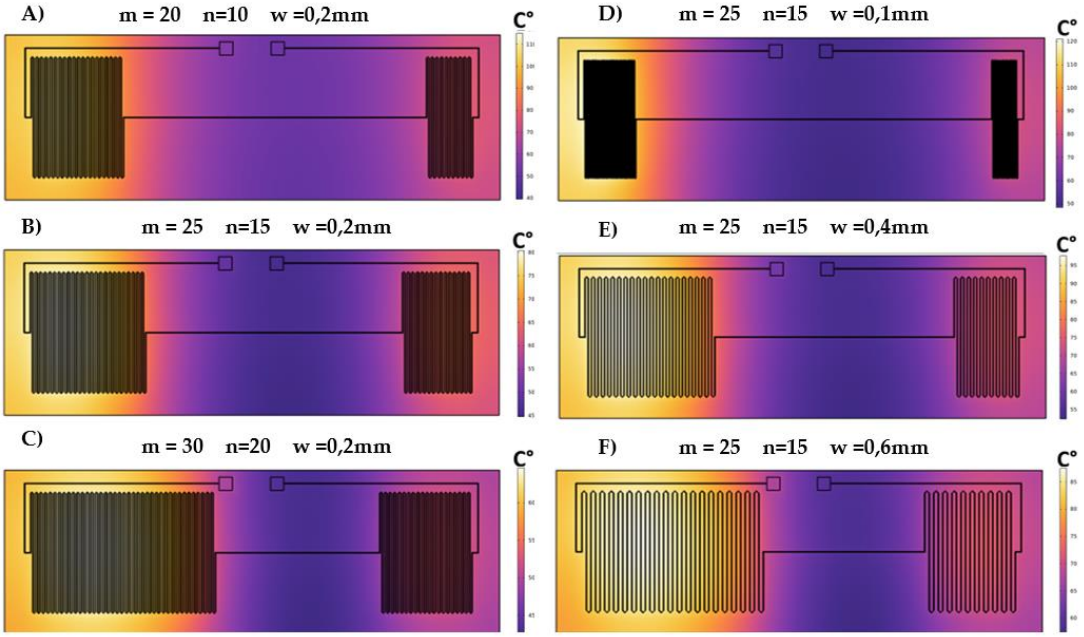

Figure 8. In silico study of different geometries. The multiphysic simulation varies the number of loops of the resistances (m and n) and the distance between loops (w).

3.2. Design and Manufacture

The printed circuit board can be seen in Figure 9.

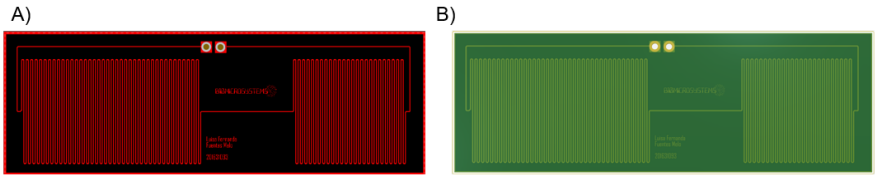

Figure 9. Final design of the microheater in ALTIUM DESIGNER 2.0 software and GERBER files A) 2D Layout Mode view of the board and B) 3D Layout Mode view of the board

Figure 10 shows the result of the manufacturing of the microheater and the integration of GP2 pins to be able to connect the circuit to a voltage source in a simpler way.

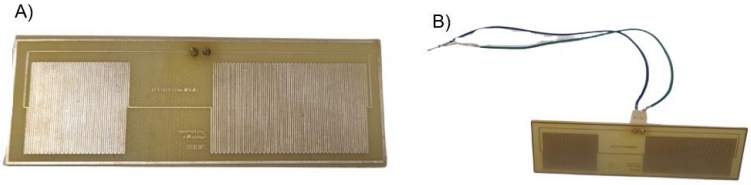

Figure 10. A) Final PCB of the microheater and B) Final assembly after soldering GP2 pins.

3.3. Theoreticalcal and experimental resistance analysis

The theoretical resistance of the microheater was calculated with equation (13).

$$R = \frac{pL}{A} \quad (13)$$

Where R is the resistance, ρ is the resistivity, L is the length, and A is the cross-sectional area. Substituting the values, an a theorical resistance of 9.96 Ω was determined (15).

$$R = \frac{0.0171\ \Omega^{mm^2}/_{m} * 2.33\ m}{0.035\ mm * 0.2\ mm} \quad (14)$$

$$R = 9.96\ \Omega \approx 10\Omega \quad (15)$$

With a multimeter, an experimental resistance of 14 Ω was measured, as show in Figure 11. The experimental resistance has a 40% increase compared to the theoretical value. The increase may be due to the purity of the material or imperfections in the manufacture.

Figure 11. Measurement with the multimeter of the practical resistance of the microheater

3.4. Theoretical and experimental thermal Characterization

Figure 12 shows the in silico thermal characterization of the selected microheater geometry, with 40 loops (m) in the resistance on the right, 25 loops (n) in the resistance on the left, and a distance between loops of 0.2 mm (w). The maximum temperature reached is 120 C and is arrived at 12V. The minimum temperature reached is 21 C and is reached with 1V. The simulations also show that the proposed geometry allows having three different temperature zones on the same plate. This will enable the board to perform temperature screening tests with microfluidic channels on the micro heater.

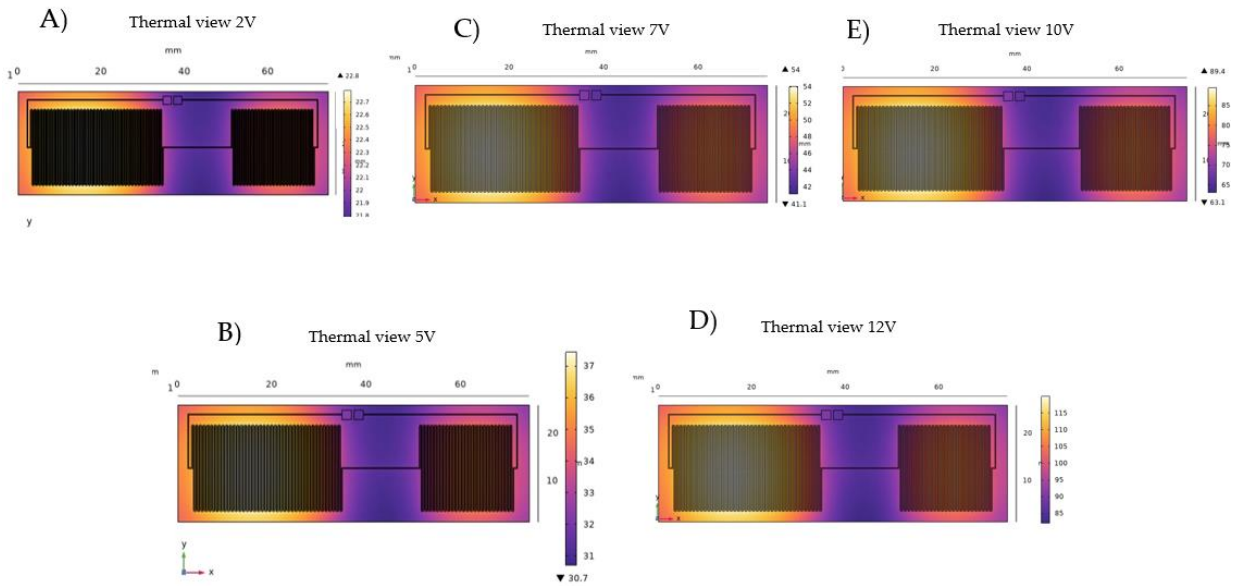

Figure 12. Simulation capture with an applied voltage of (A) 2 V (peak temperature of 22.8 °C), (B) 5 V (peak temperature of 38 °C), (C) 7 V (peak temperature of 54 °C), (D) 10V (peak temperature of 89.4 °C) and (E) 12V (peak temperature of 120 °C).

Figure 13 shows the resulting characterization of the microheater using the infrared thermometer, the behavior at one minute (blue) and two minutes (orange) at different input voltages. The curve shows a significant increase in temperature, especially after 3 V, and after reaching this point, the microheater can be considered to respond linearly to the voltage supplied to it. The average error of each measurement was calculated to the maximum and minimum temperature of the three repetitions performed in the characterization. In this case, the error range found in the 1-minute measurement is 2.157971°C positive error and 1.872464°C negative error with a ratio of 0.9718. The 2-minute error range was 1.750725°C positive error and 1.831884°C negative error with a ratio of 0.9826. Given the measurements' homogeneity, this error may be due to two factors. First, the uncertainty of the measuring equipment used, in this case, the PeakTech 4950 thermometer, and second, the human error in the calibration, for example, when measuring the temperature at the same distance and the same point of the heater.

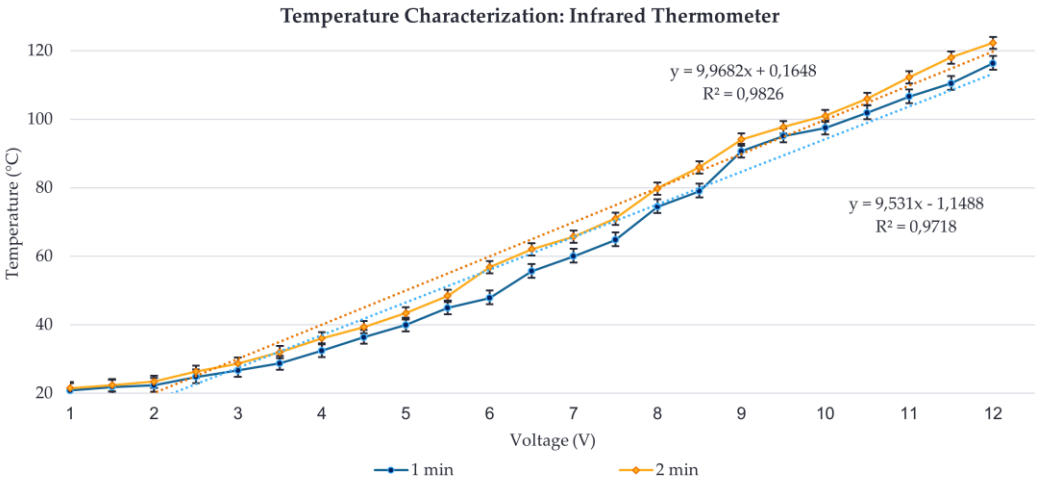

Figure 13. Results characterization process of the microheater with voltage variations of 0.5 in a range of 1 volt and 12 volts. Measurements were taken every minute and two minutes from the voltage input with an infrared thermometer.

Figure 14 shows images generated during the characterization process; each one was obtained by recording the maximum temperature value measured after a stabilization time of 30. The concentrated heat distribution within the heater zone and the temperature values correlated with the supplied voltage can be observed. It should be noted that only the left zone, which is the high-temperature zone, was evaluated to assess the system behavior. With a voltage of 2V, a temperature of 29.69°C (Figure 14A) is found at its peak, at 5V corresponds to 47.54°C (Figure 14B), at 7V corresponds to 71.2 °C (Figure 14C), at 10V corresponds to 102.14°C (Figure 14D) and 12V corresponds to 120.39°C (Figure 14E). It can be observed that the temperature distribution meets the design objective of having three different temperatures on the surface of the microheater, which confirms that the selected geometry of the heater allowed a good heat concentration zone.

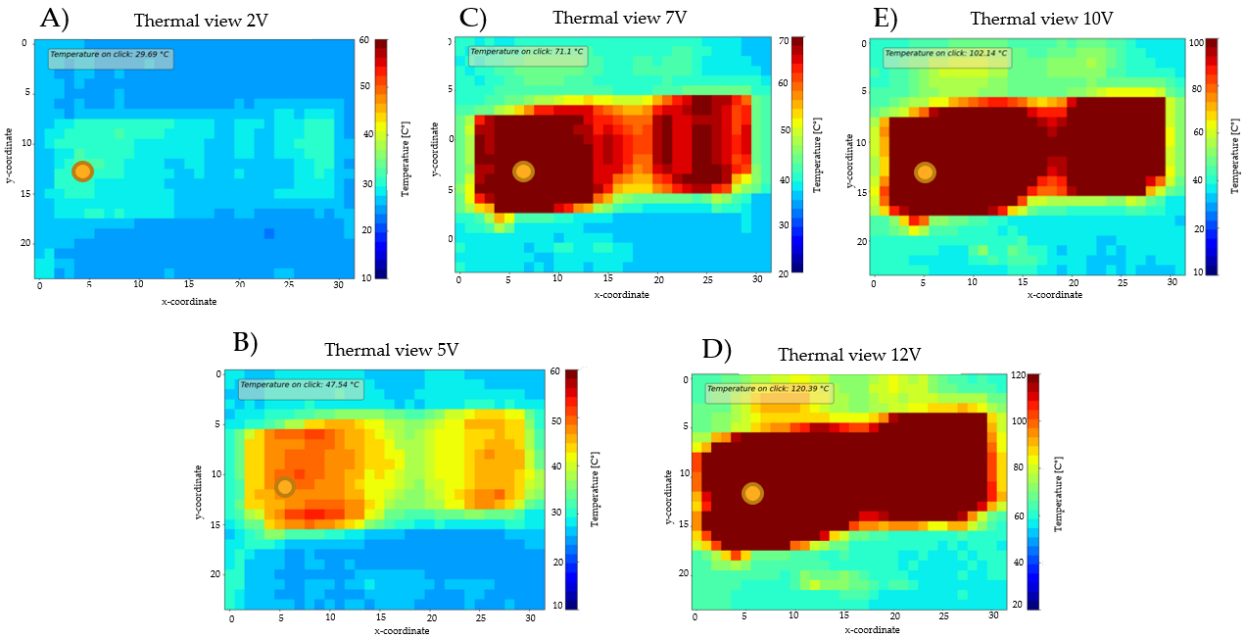

Figure 14. Image capture of the thermal camera with an applied voltage of (A) 2 V (peak temperature of 29.69 °C), (B) 5 V (peak temperature of 47.54 °C), (C) 7 V (peak temperature of 71.2 °C), (D) 10V (peak temperature of 102.14 °C) and (E) 12V (peak temperature of 120.39 °C).

The results found with the characterization in Figure 15 show similar behavior to Figure 13. Again, we see that at a voltage value of 3V, the curve takes a linear behavior that responds to the supplied voltage. The average error of each measurement with its three corresponding repetitions was calculated in the same way, and it was found that at 1 minute, the error range is 0.83777°C positive and 0.8296135°C negative with a ratio of 0.9793. The 2-minute error range is 0.813236°C positive and 0.7776329°C negative with a linear relationship of 0.9788. Comparing it with the previous measurement method, we see that the measurements were much closer to each other concerning their repetitions since the errors of both times were less than 1°C, so the homogeneity between data was much more precise and accurate. However, the errors can still have several reasons, such as the uncertainty associated with the measurement equipment of the MLX90640 thermal camera and the fact that, at some point, the measurement distance was modified or the human error associated with the point at which the temperature is measured on the surface of the microheater.

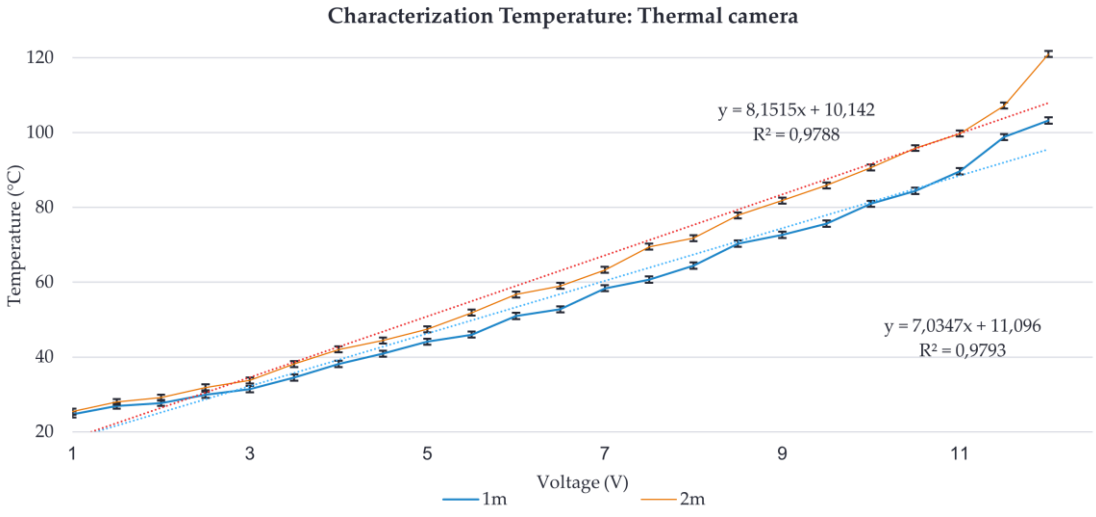

Figure 15. Results characterization process of the microheater with voltage variations of 0.5 in a range of 1 volt and 12 volts. Measurements were taken every minute and two minutes from the voltage input with a thermal camera.

Finally, a comparison of the temperature results with the two-minute characterization methods and the results obtained from the simulations was performed, as shown in Figure 16. The error from the simulation versus the two ways was 10.99955% concerning the infrared thermometer and 14.75182% concerning the thermal camera. Although the errors do not denote a significant difference, this may be due to adjustments made to the simulation, or the ideal conditions being considered may affect the physical microheater. One of these may be imperfections in the printing of the PCB tracks that may affect the resistance generated by the microheater, or the ambient temperature conditions are different in all three cases. Even so, the simulations were a good approximation of the practical results obtained after characterization.

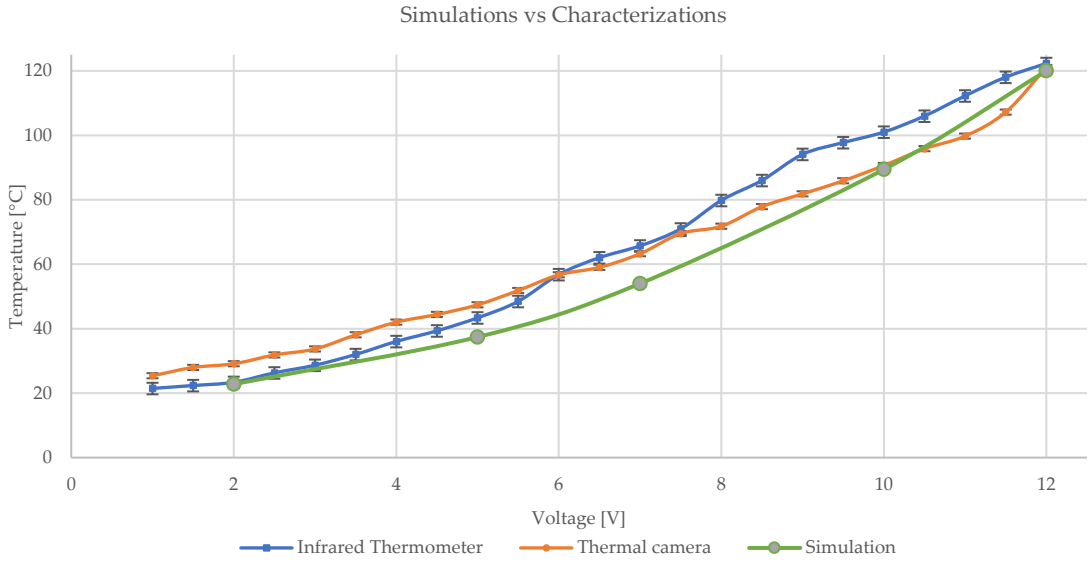

Figure 16. Results of the comparison between the temperature values measured in the infrared thermometer and thermal camera characterizations versus the results of the simulations.

Compared with the results obtained in [37],one of the advantages of the designed microheater is that it allows for reaching higher temperatures with greater precision and control. This may be due first to the materials and methods used since this microheater was made with the robustness of a printed circuit. Secondly, the microheater designed in [37] was made in the clean room laboratory of the Universidad de Los Andes, adding materials such as chromium that increased its cost and complicated its replicability. On the other hand, it was found that the response to the induced voltage presents a linear behavior and allows temperature stability concerning time compared to the uncontrolled temperature increase shown in [37]. Another advantage observed in the design is that three different temperatures are presented on the same surface so that a temperature screening can be performed for processes with various fluids and evaluate how this factor affects them. For the specific case of [37], only one fluid could be assessed in a single channel, so this new design would reduce the time needed to evaluate different channels in the same microfluidic system, and reactions requiring different temperatures could be carried out.

3.5. System stability and transfer function

Figure 17 shows the result of the microheater characterization in terms of temperature and time. These results allow us to define the time it takes for the system to stabilize and identify the behavior type when maintaining a stable power supply to design a suitable controller for future applications. The temperature stabilizes within minutes and remains stable during the time the test is performed. The average error found in the infrared thermometer measurements was in the range 1.512051°C positive and 1.472564°C negative and concerning the error range found with the thermal camera, the results were 0.811228°C positive and 1.06025°C negative. These errors may be the same as those mentioned above concerning the uncertainty of the measurement equipment used and the human error in taking that temperature at the same point and the same distance.

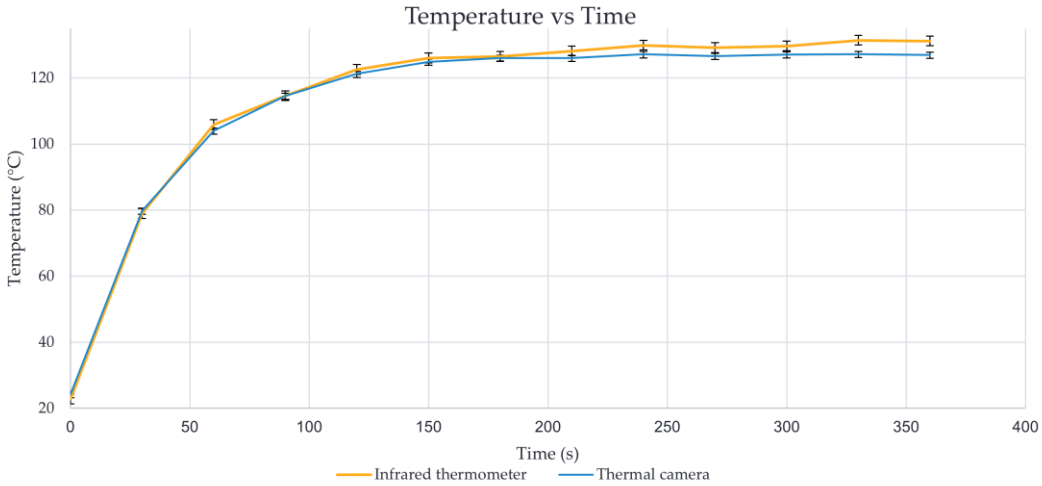

Figure 17. Results microheater´s characterization in terms of temperature vs. time at a voltage of 12V for 6 minutes with a sampling time of 30 seconds per measurement.

With these results, we proceeded to make an approximation to the transfer function of each system. For this, the data obtained from the measurements were entered into MATLAB software, and an approximation to the system was obtained with a pole and a zero and in continuous time with a sample time of 30 seconds, thus calculating the characteristic transfer function of both characterizations. In the case of the infrared thermometer characterization method, we see that the model has a fit of 96.38% concerning the data, and with the thermal camera, it has a fit of 98.64%. Both fits were more significant than 90%, as seen in Figure x13, so the calculated approximations were good for establishing the transfer functions that would facilitate the process of di-design of the temperature control.

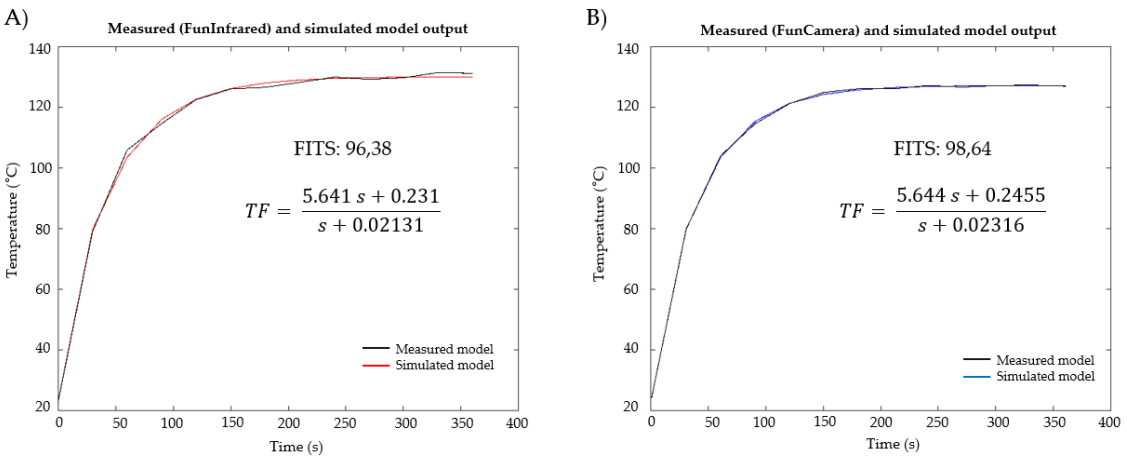

Figure 18. Transfer function results and fits of the approximations generated by each of the system characterizations.

The results obtained concerning the temperature reached were as expected and generate a reasonable basis for future work since the design and character of the microheater allow a suitable control of the temperature dissipated on its surface. Given the materials used, there is a positive temperature coefficient of resistance (PTCR) control system at this time, which is because the resistance generated by these materials would not allow an uncontrolled temperature rise. Even so, a control system is necessary to facilitate the use of the microheater and to avoid possible temperature errors that can affect the processes in the microfluidic channels. Since the system's transfer function was found in comparison with [37], a control system can be adequately designed to use the microheater in various applications with microfluidic systems, as observed in [28], which established a temperature control scheme for bioreactors.

4. Conclusions

A low-cost copper microheater printed on a FR4 substrate was designed, simulated, and characterized in a printed circuit board (PCB) process, which operates over a range of voltages from 1V to 12V to reach temperatures between 25°C to 120°C. The system also produces a maximum temperature of 122°C in measurements at an ambient temperature of ~23.5°C, with a supplied voltage of 12V and a current of 700mA. The electro-thermal results support the simulations, presenting an average error of 1.791304°C for the infrared thermometer characterization and 0.795435°C for the thermal camera characterization, both at two minutes which is the time required for system stability. Furthermore, an electro-Thermal-Mechanical mathematical model in the COMSOL Multiphysics 6.0® software (COMSOL Inc., Stockholm, Sweden) was proposed to simulate the Electromagnetic Heating of the resistance. These in silico simulations determined the micro heater's optimal geometry to generate temperatures in the desired range, presenting an error of 10.99955% with the Infrared Thermometer and 14.75182% with the Thermal Camera. Similarly, it could be concluded that the behavior related between temperature and input voltage is linear, and there is no significant increase in the system concerning time. Hence, all this led to calculating the system's transfer function to be able to design the corresponding controller for different applications in microfluidic systems in the future.

5. Patents

Supplementary Materials:

Author Contributions:

Funding

This research received no external funding

Institutional Review Board Statement

Not applicable.

Informed Consent Statement

Not applicable.

Data Availability Statement

The data and contributions presented in the study are included in the article. Further inquiries can be directed to the corresponding author.

Acknowledgments

First, I want to thank God for the opportunity he gave me to have great experiences at the university. In the same way, I do my parents, Morix Fuentes and Martha Melo, who have been my unconditional support all this time and to whom I owe everything I am. To Catalina Rangel for being the best friend I could have asked for and for supporting me at every stage in the university. To my advisor Johann Osma for providing excellent support in the project and always giving his honest opinion. To my co-advisors Cristian F. Rodriguez and Santiago Tovar for their continued support and understanding in developing this thesis and the team of laboratories of the electrical and electronic engineering department of the Universidad de Los Andes. Thanks also to all those people I cannot name now but who have been fundamental in my life: my brother Deivin, sister-in-law Sheryl, nephews Vany and Jeshua, and other friends who have taught me basic life principles.

Conflicts of Interest

The authors declare no conflict of interest.

References

[1] B. E. Rapp, "Introduction," in *Microfluidics: Modelling, Mechanics and Mathematics*, Elsevier, 2017, pp. 3–7. doi: 10.1016/B978-1-4557-3141-1.50001-0.

[2] F. Bragheri, R. Osellame, and R. Martinez Vazquez, *Microfluidics Three-Dimensional Microfabrication Using Two-photon Polymerization*. 2016.

[3] Z. E. Jeroish, K. S. Bhuvaneshwari, F. Samsuri, and V. Narayanamurthy, "Microheater: material, design, fabrication, temperature control, and applications—a role in COVID-19," *Biomed Microdevices*, vol. 24, no. 1, p. 3, Mar. 2022, doi: 10.1007/s10544-021-00595-8.

[4] J. P. Joule, "XXXVIII. *On the heat evolved by metallic conductors of electricity, and in the cells of a battery during electrolysis*," *The London, Edinburgh, and Dublin Philosophical Magazine and Journal of Science*, vol. 19, no. 124, pp. 260–277, Oct. 1841, doi: 10.1080/14786444108650416.

[5] R. G. Spruit, J. T. van Omme, M. K. Ghatkesar, and H. H. P. Garza, "A Review on Development and Optimization of Microheaters for High-Temperature <italic>In Situ</italic> Studies," *Journal of Microelectromechanical Systems*, vol. 26, no. 6, pp. 1165–1182, Dec. 2017, doi: 10.1109/JMEMS.2017.2757402.

[6] A. VanHorn and W. Zhou, "Design and optimization of a high temperature microheater for inkjet deposition," *The International Journal of Advanced Manufacturing Technology*, vol. 86, no. 9–12, pp. 3101–3111, Oct. 2016, doi: 10.1007/s00170-016-8440-8.

[7] Z. Wang *et al.*, "Robust ultrathin and transparent AZO/Ag-SnO /AZO on polyimide substrate for flexible thin film heater with temperature over 400 °C," *J Mater Sci Technol*, vol. 48, pp. 156–162, Jul. 2020, doi: 10.1016/j.jmst.2020.01.058.

[8] A. Abdeslam, K. Fouad, and A. Khalifa, "Design and optimization of platinium heaters for gas sensor applications," *Dig J Nanomater Biostruct*, vol. 15, pp. 133–141, 2020.

[9] A. Roy, M. Azadmehr, B. Q. Ta, P. Häfliger, and K. E. Aasmundtveit, "Design and Fabrication of CMOS Microstructures to Locally Synthesize Carbon Nanotubes for Gas Sensing," *Sensors*, vol. 19, no. 19, p. 4340, Oct. 2019, doi: 10.3390/s19194340.

[10] G. Velmathi, N. Ramshanker, and S. Mohan, "Design, Electro-Thermal simulation and geometrical optimization of double spiral shaped microheater on a suspended membrane for gas sensing," in *IECON 2010 - 36th Annual Conference on IEEE Industrial Electronics Society*, Nov. 2010, pp. 1258–1262. doi: 10.1109/IECON.2010.5675550.

[11] C. Zheng, G. P. S. Balasubramanian, Y. Tan, A. M. Maniatty, R. Hull, and J. T. Wen, "Simulation, Microfabrication, and Control of a Microheater Array," *IEEE/ASME Transactions on Mechatronics*, vol. 22, no. 4, pp. 1914–1919, Aug. 2017, doi: 10.1109/TMECH.2017.2650682.

[12] Y. Zhu, A. Bui, H. Jin, S. Nahavandi, E. C. Harvey, and I. D. Sutalo, "Thermal modeling of a microheater in a microchannel chip," Dec. 2005, p. 60361Y. doi: 10.1117/12.660972.

[13] S. Yu, S. Wang, M. Lu, and L. Zuo, "A novel polyimide based micro heater with high temperature uniformity," *Sens Actuators A Phys*, vol. 257, pp. 58–64, Apr. 2017, doi: 10.1016/j.sna.2017.02.006.

[14] J.-L. Lin, S.-S. Wang, M.-H. Wu, and C.-C. Oh-Yang, "Development of an Integrated Microfluidic Perfusion Cell Culture System for Real-Time Microscopic Observation of Biological Cells," *Sensors*, vol. 11, no. 9, pp. 8395–8411, Aug. 2011, doi: 10.3390/s110908395.

[15] J. M. Son, J. H. Lee, J. Kim, and Y. H. Cho, "Temperature distribution measurement of Au micro-heater in microfluidic channel using IR microscope," *International Journal of Precision Engineering and Manufacturing*, vol. 16, no. 2, pp. 367–372, Feb. 2015, doi: 10.1007/s12541-015-0048-7.

[16] J.-W. Han and M. Meyyappan, "A Built-In Temperature Sensor in an Integrated Microheater," *IEEE Sens J*, vol. 16, no. 14, pp. 5543–5547, Jul. 2016, doi: 10.1109/JSEN.2016.2569445.

[17] J. Kang *et al.*, "Temperature control of micro heater using Pt thin film temperature sensor embedded in micro gas sensor," *Micro and Nano Systems Letters*, vol. 5, no. 1, p. 26, Dec. 2017, doi: 10.1186/s40486-017-0060-z.

[18] T. Guan and R. Puers, "Thermal analysis of a Ag/Ti based microheater," *Procedia Eng*, vol. 5, pp. 1356–1359, 2010, doi: 10.1016/j.proeng.2010.09.366.

[19] C. Offenzeller, M. Knoll, T. Voglhuber-Brunnmaier, M. A. Hintermuller, B. Jakoby, and W. Hilber, "Fully Screen Printed Thermocouple and Microheater Applied for Time-of-Flight Sensing in Microchannels," *IEEE Sens J*, vol. 18, no. 21, pp. 8685–8692, Nov. 2018, doi: 10.1109/JSEN.2018.2868161.

[20] G. Petrucci *et al.*, "Thermal characterization of thin film heater for lab-on-chip application," in *2015 XVIII AISEM Annual Conference*, Feb. 2015, pp. 1–4. doi: 10.1109/AISEM.2015.7066835.

[21] S. K. Tiwari, S. Bhat, and K. K. Mahato, "Design and fabrication of screen printed microheater," *Microsystem Technologies*, vol. 24, no. 8, pp. 3273–3281, Aug. 2018, doi: 10.1007/s00542-018-3821-6.

[22] J. Nie, Y. Zhao, and N. Peng, "Multichannel oscillatory-flow PCR micro-fluidic chip with controllable temperature gradient," *Microsystem Technologies*, vol. 21, no. 1, pp. 41–48, Jan. 2015, doi: 10.1007/s00542-014-2077-z.

[23] S. Jeong *et al.*, "Portable low-power thermal cycler with dual thin-film Pt heaters for a polymeric PCR chip," *Biomed Microdevices*, vol. 20, no. 1, p. 14, Mar. 2018, doi: 10.1007/s10544-018-0257-9.

[24] M. Megayanti, C. Panatarani, and I. M. Joni, "Development of microheaters for gas sensor with an AT-Mega 8535 temperature controller using a PWM (pulse width modulation) method," 2016, p. 030046. doi: 10.1063/1.4943741.

[25] J. Wu, W. Cao, W. Wen, D. C. Chang, and P. Sheng, "Polydimethylsiloxane microfluidic chip with integrated microheater and thermal sensor," *Biomicrofluidics*, vol. 3, no. 1, p. 012005, Mar. 2009, doi: 10.1063/1.3058587.

[26] R. Phatthanakun, P. Deekla, W. Pummara, C. Sriphung, C. Pantong, and N. Chomnawang, "Design and fabrication of thin-film aluminum microheater and nickel temperature sensor," in *2012 7th IEEE International Conference on Nano/Micro Engineered and Molecular Systems (NEMS)*, Mar. 2012, pp. 112–115. doi: 10.1109/NEMS.2012.6196735.

[27] S. Singh, D. K. Sharma, K. Kishore, B. A. Botre, and S. A. Akbar, "Modeling, Simulation, and Implementation of Fast Settling Switched PI Controller for MOX Integrated Pt Microheater," *IEEE Sens J*, vol. 18, no. 20, pp. 8549–8557, Oct. 2018, doi: 10.1109/JSEN.2018.2867233.

[28] M. N. H. Zainal Alam, A. A. A. Moghadam, and A. Kouzani, "Establishment of temperature control scheme for microbioreactor operation using integrated microheater," *Microsystem Technologies*, vol. 21, no. 2, pp. 415–428, Feb. 2015, doi: 10.1007/s00542-014-2088-9.

[29] N. Lovecchio *et al.*, "Thermal control system based on thin film heaters and amorphous silicon diodes," in *2015 6th International Workshop on Advances in Sensors and Interfaces (IWASI)*, Jun. 2015, pp. 277–282. doi: 10.1109/IWASI.2015.7184977.

[30] M. Mirasoli *et al.*, "On-chip LAMP-BART reaction for viral DNA real-time bioluminescence detection," *Sens Actuators B Chem*, vol. 262, pp. 1024–1033, Jun. 2018, doi: 10.1016/j.snb.2018.02.086.

[31] D. Moschou *et al.*, "All-plastic, low-power, disposable, continuous-flow PCR chip with integrated microheaters for rapid DNA amplification," *Sens Actuators B Chem*, vol. 199, pp. 470–478, Aug. 2014, doi: 10.1016/j.snb.2014.04.007.

[32] J.-S. Hwang, S.-Y. Kim, Y.-S. Kim, H.-J. Song, C.-Y. Park, and J.-D. Kim, "Implementation of PCB-Based PCR Chip Using Double-Sided Tape," *International Journal of Control and Automation*, vol. 8, no. 2, pp. 117–124, Feb. 2015, doi: 10.14257/ijca.2015.8.2.12.

[33] N. Holt, L. G. Marques, A. van Horn, M. Montazeri, and W. Zhou, "Fabrication and control of a microheater array for Microheater Array Powder Sintering," *The International Journal of Advanced Manufacturing Technology*, vol. 95, no. 1–4, pp. 1369–1376, Mar. 2018, doi: 10.1007/s00170-017-1316-8.

[34] F. Cui *et al.*, "Design and experiment of a PDMS-based PCR chip with reusable heater of optimized electrode," *Microsystem Technologies*, vol. 23, no. 8, pp. 3069–3079, Aug. 2017, doi: 10.1007/s00542-016-3064-3.

[35] T. Pardy, I. Tulp, C. Kremer, T. Rang, and R. Stewart, "Integrated self-regulating resistive heating for isothermal nucleic acid amplification tests (NAAT) in Lab-on-a-Chip (LoC) devices," *PLoS One*, vol. 12, no. 12, p. e0189968, Dec. 2017, doi: 10.1371/journal.pone.0189968.

[36] M. Horade, M. Kojima, K. Kamiyama, Y. Mae, and T. Arai, "Development of a Novel 2-Dimensional Micro-Heater Array Device with Regional Selective Heating," *Mechanical Engineering Research*, vol. 6, no. 1, p. 66, Apr. 2016, doi: 10.5539/mer.v6n1p66.

[37] S. Tovar, C. A. Hernández, and J. F. Osma, "Design, Simulation, and Fabrication of a Copper–Chrome-Based Glass Heater Integrated into a PMMA Microfluidic System," *Micromachines (Basel)*, vol. 12, no. 9, p. 1067, Sep. 2021, doi: 10.3390/mi12091067.